Effects of Alkali Halides on the Thermal Decompositions of Poly(methyl methacrylate) and Poly(2-hydroxy ethyl methacrylate)

THEKKEKALATHIL M. CHANDRASEKHAR and ROBERT L. WHITE*

Department of Chemistry and Biochemistry, University of Oklahoma, Norman, Oklahoma 73019

SYNOPSIS

The effects of alkali halides on the nonoxidative thermal degradations of poly(methyl methacrylate) and poly(2-hydroxy ethyl methacrylate) are described. The magnitudes of the effects of various alkali halides on polymer thermal degradations were found to depend on the salt and the polymer. Mass spectrometric analysis of volatiles evolved during polymer degradation detected alkyl halides formed by reactions between the salts and polymers. Compared to poly(methyl methacrylate), more alkyl halide was evolved from samples containing alkali halides and poly(2-hydroxy ethyl methacrylate). To varying degrees, salts also catalyzed ester decomposition reactions for this polymer. Infrared spectroscopic analysis results showed that carboxylate salts, carbonate, and carbon monoxide were formed by heating polymer/salt mixtures. © 1996 John Wiley & Sons, Inc.

INTRODUCTION

Polymers are employed as binders to form ceramic green bodies that are subsequently fired to produce ceramic products. Ideally, polymer binders decompose (burnout) completely below temperatures required for ceramic sintering. Although complete decomposition can usually be achieved in oxidative burnout atmospheres, incomplete binder decomposition may occur in the inert or reductive atmospheres that are often employed to avoid oxidation of cofired metals in the production of integrated circuit substrates.[1-5] Compared to other commonly used polymer binders, the thermal properties of acrylic and methacrylic copolymers are well suited for these applications because they decompose more completely and at lower temperature in nonoxidative environments. Another advantage to the use of acrylic and methacrylic copolymers as ceramic binders is that they can be applied as aqueous solutions or emulsions, so that the environmental impact of large scale industrial applications is minimal when these polymers are employed.

If significant quantities of polymer binder residue remain above temperatures at which ceramic sintering begins, flaws in ceramic end products may result. It is known that inorganic oxides can interact with polymer binders during burnout and that these interactions affect binder thermal degradation.[6-12] It has, therefore, been useful to examine the effects of inorganic oxides on the nonoxidative thermal degradations of polymer binders used in electronics industry applications. In our previous study of the effects of silica on the nonoxidative thermal degradation of a multifunctional polymer containing acrylic and methacrylic moieties,[12] we found that potassium bromide that was mixed with polymers to prepare samples for infrared analysis had a pronounced effect on the thermal degradation of the polymer binder. Because studies of the effects of polar materials such as alkali halides on the thermal degradations of polymer binders may be useful for characterizing the interactions that occur between polymers and inorganic oxide Lewis sites (acidic and basic) during the initial stages of ceramic sintering, we have investigated this phenomenon in greater detail. In this article, the effects of a variety of alkali

* To whom correspondence should be addressed.

Journal of Applied Polymer Science, Vol. 60, 1209–1219 (1996)
 CCC 0021-8995/96/081209-11

halides on the thermal degradation processes of poly(methyl methacrylate) (PMMA) and poly(2-hydroxy ethyl methacrylate) (PHEMA) are described. PMMA and PHEMA were selected for study because the functionalities present in these polymers are commonly employed in copolymers used by the microelectronics industry for nonoxidative ceramic sintering.

EXPERIMENTAL

The PMMA (MW = 350,000) and PHEMA (MW = 300,000) polymers and the alkali halides used in this study were purchased from Aldrich Chemical Co. (Milwaukee, WI) and were used without further purification. Both polymers were made by free radical polymerization. PMMA was received in the form of a fine powder, whereas PHEMA was obtained as larger particles and was ground into a fine powder prior to analyses. Samples containing the polymers and alkali halides were made by mixing the polymers and salts in a 1 : 1 weight ratio and grinding the mixture.

Pyrolysis-GC experiments were performed by using a microfurnace pyrolyzer built in our laboratory.[13] The pyrolysis oven was interfaced to a Hewlett Packard (Palo Alto, CA) 5980A capillary gas chromatograph. A 25 m × 0.32 mm i.d. Hewlett Packard Ultra-1 column with 0.52 μm crosslinked methyl silicone gum stationary phase was used for separations. A He carrier gas flow rate of 4 mL/min and a temperature program starting with a 2 min isothermal period at 50°C followed by a 10°C/min ramp to 250°C were employed for separations. GC/MS detection of pyrolysis products was facilitated by interfacing the gas chromatograph to a Hewlett Packard 5985 quadrupole mass spectrometer. Electron impact mass spectra were acquired at a rate of 25 spectra/min by using a 70 eV ionization potential and scanning from m/z 10 to m/z 300. Mass spectral library searches employed a 36,218 spectra NBS mass spectral library. GC/FT-IR measurements were obtained by interfacing a Mattson Instruments Inc. (Madison, WI) Sirius 100 FT-IR to the Hewlett Packard 5980A gas chromatograph via a light pipe interface constructed in our laboratory. GC/FT-IR spectra were acquired at 8 cm^{-1} resolution at a rate of 20 spectra/min. Infrared spectra were searched against a 3300 spectra EPA vapor phase infrared library.

Thermogravimetric analyses were performed with a DuPont (Wilmington, DE) model 951 TG analyzer. TG–MS measurements were made by connecting the gas outlet of the TG analyzer to a Hewlett Packard (Palo Alto, CA) 5985 quadrupole mass spectrometer by using a Scientific Glass Engineering Inc. (Austin, TX) MCVT-1–50 variable splitting valve. The TG–MS interface was maintained at 250°C by using heating tapes. The He TG purge gas flow rate was 50 mL/min. TG–MS results were obtained by heating approximately 10 mg samples from 50°C to 550°C at a rate of 10°C/min. TG–MS mass spectra were acquired by using 70 eV electron bombardment ionization and scanning from m/z 10 to m/z 200 at a rate of 3 spectra/min. Ion source pressure was maintained at 2×10^{-5} Torr during TG–MS measurements.

The VT-DRIFTS apparatus and procedures for acquiring variable temperature diffuse reflectance infrared spectra have been described previously.[14–18] About 15 mg quantities of samples were placed in the sample holder for measurements. The DRIFTS sample chamber He purge gas flow rate was maintained at 10 mL/min during VT-DRIFTS measurements by using an Edwards High Vacuum, Inc. (Grand Island, NY) model 825 mass flow controller. A heating rate of 10°C/min from 50 to 550°C was used for VT-DRIFTS measurements. DRIFTS measurements were made at a rate of 1 spectrum/min over the 4000 to 750 cm^{-1} range at a resolution of 8 cm^{-1}.

RESULTS

Neat Polymers

In order to unequivocally attribute changes in polymer thermal properties to effects of alkali halides, it was first necessary to characterize the neat polymers by using the same analysis techniques that would be used to study polymer/salt mixtures. Consequently, neat PMMA and PHEMA samples were analyzed by pyrolysis–GC/MS, pyrolysis–GC/FT-IR, TG–MS, and VT-DRIFTS.

Because the PMMA and PHEMA polymers used in this study were synthesized by free radical polymerization, some polymer chains contained head-to-head linkages and vinylidene chain ends caused by radical combination and radical disproportionation, respectively.[19–21] During TG analyses in He, both neat polymers exhibited decompositions with no observable residue. As shown in Figure 1(a), sample weight loss during the thermal degradation of PMMA occurred in three distinct steps. The first

step, attributed to unzipping after initial cleavage of head-to-head linkages,

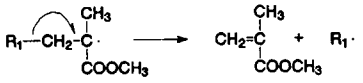

reached a maximum weight loss rate at 187°C and resulted in a ~ 5% total weight loss. The second step, attributed to initial β-scission at vinylidene chain ends followed by unzipping, reached a maximum weight loss rate at 300°C and was characterized by a 20% sample weight loss.

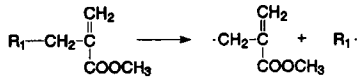

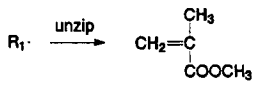

The third degradation step, due to unzipping after random chain cleavage, reached a maximum weight loss rate at 379°C and resulted in the decomposition of the remaining polymer.

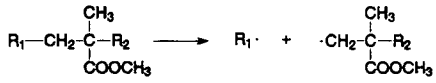

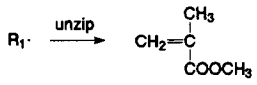

Mass spectra acquired during TG–MS analysis of PMMA confirmed that the primary volatile product produced during each weight loss stage was methyl methacrylate monomer. In fact, the ion signal temperature profiles for m/z 100 (monomer molecular ion), m/z 69 (base peak in the mass spectrum of methyl methacrylate), and the total ion current resembled the derivative of the weight loss curve in Figure 1(a).

The weight loss curve for the thermal degradation of PHEMA [Fig. 1(b)] consisted of four stages. The

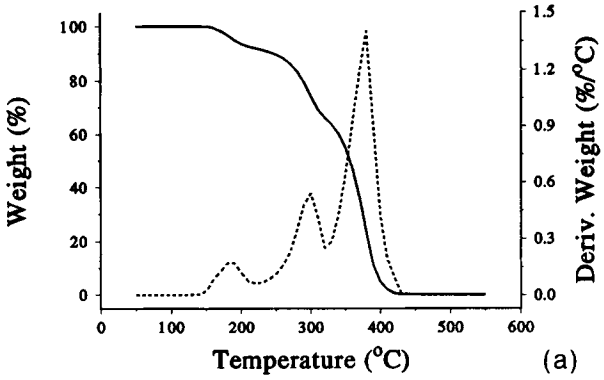

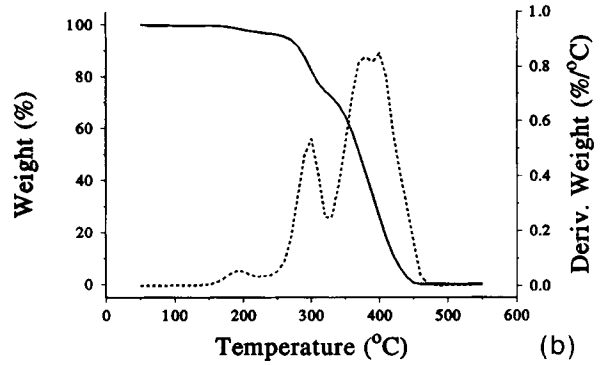

Figure 1 Weight loss curves (solid lines) and derivative weight loss curves (dashed lines) obtained by TG–MS analysis of (a) neat PMMA and (b) neat PHEMA.

relative magnitude and the widths of PHEMA derivative weight peaks detected at 198 and 301°C were similar to those for the two PMMA weight loss steps that occurred at comparable temperatures. TG–MS mass spectra acquired during these weight loss steps indicated that the primary volatile product was monomer (2-hydroxy ethyl methacrylate). These first two PHEMA weight loss steps were likely caused by the same processes attributed to the first two PMMA weight loss steps: unzipping after polymer cleavage at head-to-head linkages and at vinylidene chain ends, respectively. Unlike PMMA, the weight loss curve for PHEMA indicated that at least two thermal degradation processes occurred between 350 and 450°C. TG–MS mass spectra obtained between 350 and 450°C during PHEMA thermal degradation exhibited changes with temperature, which confirmed that more than one volatile product was produced in this temperature range. As shown in Figure 2, the m/z 69 ion signal temperature profile obtained by TG–MS analysis of

PHEMA exhibited four maxima located near the same temperatures as the derivative weight curve maxima shown in Figure 1(b). Because m/z 69 is the base peak in mass spectra of alkyl methacrylates, the m/z 69 ion signal temperature profile in Figure 2 suggests that alkyl methacrylates were evolved during each of the four PHEMA weight loss steps depicted in Figure 1(b). In addition, the m/z 62 (ethylene glycol molecular ion) and m/z 86 (methacrylic acid molecular ion) ion signal temperature profiles (Fig. 2) suggest that ethylene glycol and methacrylic acid were produced between 350 and 450°C. Ethylene glycol can be formed by pendant group elimination reactions.[22]

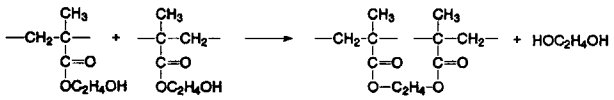

Unzipping of the resulting crosslinked polymer can produce ethylene glycol dimethacrylate.

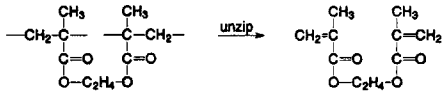

Methacrylic acid can be formed by unzipping of polymer segments that have undergone ester decomposition, which results in the formation of ethenol ($CH_2{=}CHOH$, m/z 44)[23].

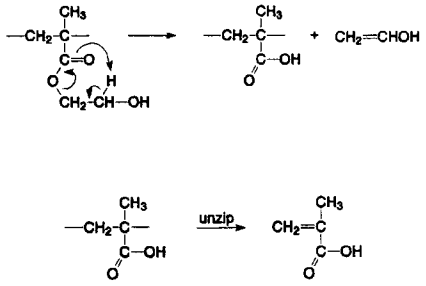

Pyrolysis–GC/MS and pyrolysis–GC/FT-IR analyses of neat PHEMA at 500°C confirmed that significant quantities of ethylene glycol and ethylene glycol dimethacrylate were formed along with some ethenol and methacrylic acid. Although some of the m/z 69 ($CH_2{=}C(CH_3)CO^+$) ion signal detected between 350 and 450°C by TG–MS was undoubtedly due to ethylene glycol dimethacrylate, the ethylene glycol dimethacrylate molecular ion at m/z 198 was too weak to be detected by TG–MS.

Diffuse reflectance infrared spectra for PMMA and PHEMA are shown in Figure 3. The PMMA infrared spectrum contains strong absorptions at

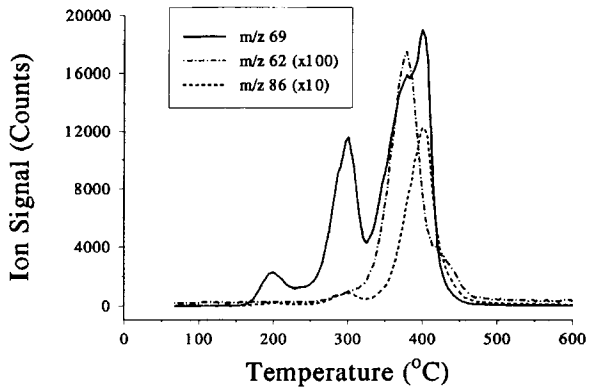

Figure 2 Ion signal temperature profiles obtained by TG–MS analysis of neat PHEMA.

2950 and 1730 cm^{-1} that correspond to aliphatic C—H and carbonyl C=O stretches, respectively. Several medium to strong absorptions in the 1610–1300 cm^{-1} region were due to CH_3 and CH_2 deformations, and a strong band at 1260 cm^{-1} was due to mixing between CH_3 rock and C—C stretching vibrations.[24] Two strong bands at 1077 and 1000 cm^{-1} were due to C—O—C asymmetric and symmetric stretching vibrations, respectively. The small OH stretching vibration absorption at 3450 cm^{-1} was most likely due to methacrylic acid impurities in polymer chains. When the PMMA sample was heated, the absorbances of all of the infrared bands decreased proportionately as the polymer decomposed, which is consistent with TG–MS evidence that polymer unzipping to form monomer was the primary thermal decomposition process.

The infrared spectrum of PHEMA contained strong absorptions near 3500 and 2950 cm^{-1} that corresponded to O—H and C—H stretching vibrations, respectively, and a sharp intense band at 1730 cm^{-1} corresponding to the C=O stretching vibration. In addition, medium to strong bands observed in the 1610–1300 cm^{-1} region were due to CH_3 and CH_2 deformations, and absorptions in the 1300–1000 cm^{-1} region were due to C—O—C stretching vibrations. Like the PMMA sample, there was a gradual decrease in the intensity of all of these bands when the sample was heated.

Polymer/Salt Mixtures

Figure 4 shows derivative weight loss curves obtained by TG–MS analysis of each of the PMMA/salt mixtures. With the exceptions of the PMMA/LiI and PMMA/CsF samples, the PMMA/salt mixtures exhibited three-step weight losses that re-

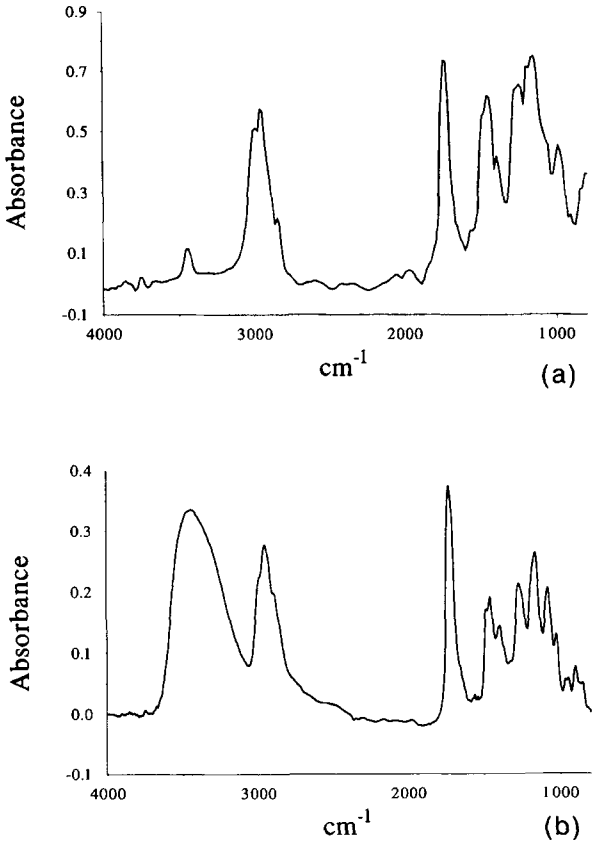

Figure 3 Infrared spectra obtained at 50°C by VT-DRIFTS analysis of (a) neat PMMA and (b) neat PHEMA.

sembled that for neat PMMA [Fig. 1(a)]. The two peaks apparent below 150°C for the PMMA/LiI sample in Figure 4(a) were caused by weight loss attributed to water desorption. The TG–MS derivative weight loss peak that maximized below 200°C for neat PMMA and the other PMMA/salt mixtures maximized above 200°C for the PMMA/LiI sample. TG–MS mass spectra revealed that water evolution from the PMMA/CsF mixture between 150 and 250°C contributed to the shape of the first derivative weight loss peak for this sample. Mass spectra obtained during TG–MS analysis indicated that methyl methacrylate monomer was the primary volatile product formed by thermal decomposition of the PMMA/salt mixtures. In addition, some methyl halide was detected for all but the PMMA/LiF sample. Methyl halides were formed by reactions between PMMA and the salts.

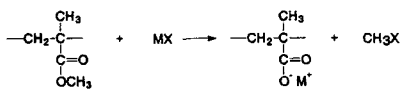

The amount of methyl halide generated by heating PMMA/salt mixtures was very small. Sample masses at 600°C for these 1 : 1 (w/w) PMMA/salt mixtures were typically about 50% of the initial

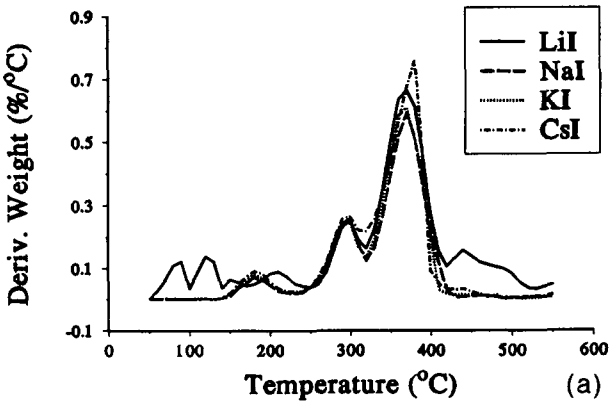

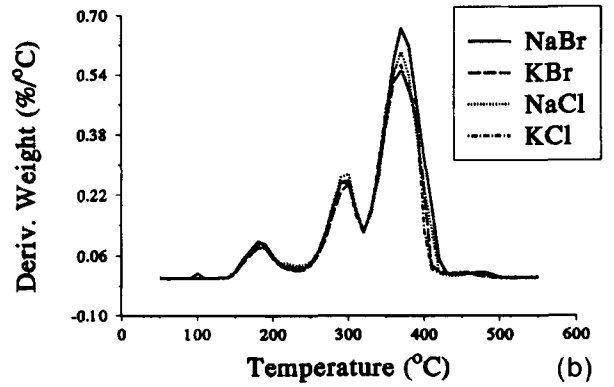

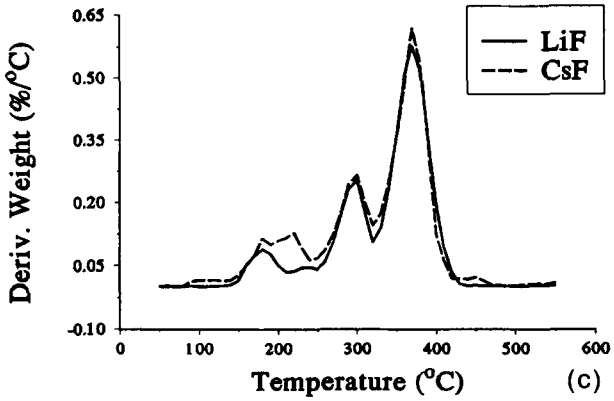

Figure 4 Derivative weight loss curves obtained by TG–MS analysis of PMMA/salt mixtures.

sample mass, indicating that sample weight loss was primarily associated with the loss of polymer. Temperatures corresponding to methyl halide molecular ion maxima derived from TG–MS analysis of PMMA/salt mixtures are compiled in Table I. The PMMA/alkali iodide mixtures produced the most methyl halide and much more methyl halide was detected for the PMMA/LiI mixture than any other sample. Although some methyl iodide was detected for the PMMA/alkali iodide mixtures at temperatures below 350°C, the highest methyl iodide evolution rates for these samples were above the temperature at which the maximum rate of monomer evolution was detected for neat PMMA (i.e., above 379°C).

At temperatures high enough to remove adsorbed water from alkali halides, VT-DRIFTS spectra obtained for the PMMA/salt mixtures contained many of the same features observed in neat PMMA spectra. In addition, some absorbance bands that were not present in neat PMMA spectra were observed in PMMA/salt spectra. Figure 5 shows infrared absorbance band intensity temperature profiles for some of these bands and the ester carbonyl stretching vibration (1730 cm^{-1}) along with m/z 69 (alkyl methacrylate base peak) and m/z 142 (CH_3I molecular ion) ion signal temperature profiles derived from VT-DRIFTS and TG–MS analysis of the PMMA/NaI sample. VT-DRIFTS spectra obtained for most of the other PMMA/salt mixtures contained the same infrared bands, and these bands exhibited temperature dependencies similar to those depicted in Figure 5. A band at 1560 cm^{-1}, representative of carboxylate,[7,12,25] was found in spectra acquired above 275°C. At higher temperatures, infrared absorbance bands at 2166, 1428, and 872 cm^{-1} were detected. The broad 1428 cm^{-1} band and the sharp band at 872 cm^{-1} were characteristic of carbonate formation.[26,27] The infrared band at 2166 cm^{-1} was most likely due to adsorbed carbon monoxide produced by carboxylate decompositions. The m/z 69 ion signal temperature profile exhibited three maxima and resembled the derivative weight loss curve shown in Figure 1(a). Although the m/z 142 ion signal maximized at 409°C, m/z 142 was first detected near 250°C, which coincided with the appearance of the 1560 cm^{-1} carboxylate infrared absorbance band in VT-DRIFTS spectra.

Unlike PMMA, the derivative weight loss curves for PHEMA/salt mixtures were quite different from the neat PHEMA curve. As shown in Figure 6, none of the PHEMA/salt derivative weight loss curves resembled that for neat PHEMA [Fig. 1(b)]. With the exception of the PHEMA/LiF sample, none of the derivative weight loss curves for the PHEMA/

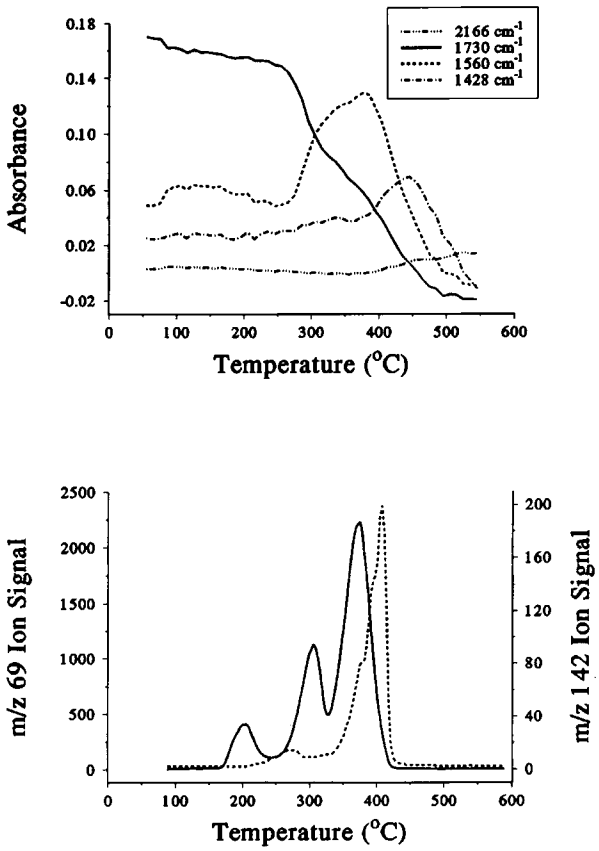

Figure 5 Infrared absorbance band intensity temperature profiles (top) and ion signal temperature profiles (bottom) for m/z 69 (solid line) and m/z 142 (dashed line) obtained by VT-DRIFTS and TG–MS analysis of a PMMA/NaI mixture.

Table I TG-MS Methyl Halide Molecular Ion Maxima for PMMA/Salt Mixtures

Salt	Peak Maxima (°C)[a]		
LiI	211 (33)	295 (18)	380 (100)
NaI	262 (7)		409 (100)
KI		306 (17)	391 (100)
CsI		306 (57)	382 (100)
NaBr			359
KBr			376
NaCl			408
KCl			389
LiF			—
CsF			382

[a] Numbers in parentheses denote relative peak intensities when multiple peaks were detected.

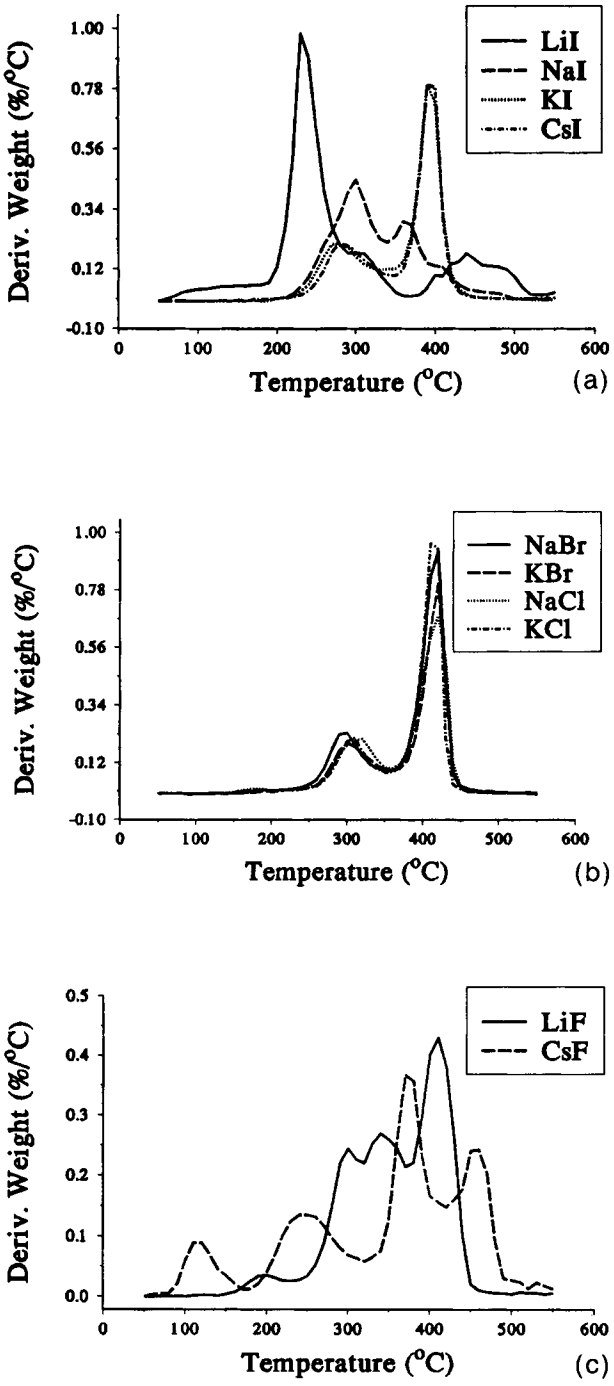

Figure 6 Derivative weight loss curves obtained by TG–MS analysis of PHEMA/salt mixtures.

salt mixtures contained a peak near 180°C representing unzipping after head-to-head linkage cleavage. Like the PMMA/salt mixtures, the effects of alkali iodides were particularly significant. The thermal behavior of the PHEMA/LiI sample was much different from the other PHEMA/salt mixtures. For example, most of the PHEMA/LiI sample weight loss occurred between 200 and 250°C, TG–MS mass spectra revealed that the primary volatile product evolved during this temperature range was 2-hydroxy ethyl iodide ($HOCH_2CH_2I$), and TG–MS weight loss curves revealed that residual sample masses measured at 600°C were well below 50%. Compared to the PHEMA/LiI sample, less 2-hydroxy ethyl halide was detected during the thermal decompositions of the other PHEMA/salt mixtures.

Table II TG-MS 2-Hydroxy Ethyl Halide Molecular Ion Maxima for PHEMA/Salt Mixtures

Salt	Peak Maxima (°C)[a]		
LiI	229		
NaI	255 (100)	296 (73)	
KI	255 (100)		408 (60)
CsI	260 (100)		396 (16)
NaBr		284 (21)	415 (100)
KBr			414
NaCl			415
KCl			411
LiF			420
CsF	230		

[a] Numbers in parentheses denote relative peak intensities when multiple peaks were detected.

The PHEMA/alkali bromide and PHEMA/alkali chloride samples exhibited similar derivative weight loss curves containing peaks near 300 and 400°C. TG–MS mass spectra indicated that both of these peaks resulted primarily from monomer evolution. The PHEMA/LiF derivative weight loss curve contained four peaks with maxima near 190, 290, 330, and 410°C. TG–MS mass spectra indicated that all four of these weight loss peaks were primarily the result of monomer evolution. The CsF derivative weight loss curve also exhibited four peaks, but their maxima were located at 120, 240, 375, and 460°C. TG–MS mass spectra indicated that the 120°C peak was due to water desorption, the 240°C derivative weight loss peak correlated with the formation of ethenol and 2-hydroxy ethyl fluoride, the 375°C peak was primarily due to monomer evolution, and the

460°C peak resulted from carbon dioxide formation. As shown by Table II, the temperatures corresponding to the maximum rate of alkyl halide production for the PHEMA/alkali iodide and PHEMA/CsF samples ranged from 229 to 260°C. Compared to PMMA/salt samples, the quantities of alkyl halide produced from PHEMA/salt mixtures were much higher.

Figure 7 shows PHEMA/NaI infrared absorbance band intensity temperature profiles for the same bands characterized in Figure 5 for the PMMA/NaI mixture along with m/z 69 and m/z 172 (2-hydroxy ethyl iodide molecular ion) ion signal temperature profiles. Like the PMMA/NaI results shown in Figure 5, the 1560 cm^{-1} carboxylate band appeared in infrared spectra near 250°C and carbonate and carbon monoxide bands appeared above 400°C. Unlike the PMMA/NaI results, the PHEMA/NaI m/z 69 ion signal temperature profile did not resemble the derivative weight loss curve derived from TG–MS analysis of neat PHEMA, and most of the alkyl halide produced by heating the PHEMA/NaI mixture evolved below 300°C.

DISCUSSION

The fact that the thermal degradation of PMMA was only slightly affected by the alkali halides, whereas PHEMA thermal decomposition was dramatically changed, illustrates the important role of pendant group functionalities in the thermal degradation of methacrylic polymers. The amount of alkyl halide produced from PMMA/salt samples was very small and the contribution from this process to the overall weight loss of PMMA/salt mixtures was negligible. In contrast, the effects of the alkali halides on the PHEMA thermal degradation processes were significant. The PHEMA/salt mixtures generated more alkyl halides because ester —O—(CH_2) bonds were weaker than —O—(CH_3) bonds and were more easily broken by interactions with polar salt surfaces.

TG–MS evidence for PHEMA unzipping following head-to-head linkage scission was only obtained for the PHEMA/LiF sample. Strong interactions between PHEMA and the other alkali halides apparently prevented unzipping from occurring. Because the primary difference between PMMA and PHEMA was in the functionality of the pendant groups, it was likely that the PHEMA hydroxyls were involved in polymer–salt interactions that prevented PHEMA unzipping below 200°C for all except the PHEMA/LiF mixture. Apparently, thermal degradation initiated by head-to-head linkage scission was suppressed because the resulting radicals were held in place by cage formation. A similar "cage effect" has been observed for high molecular weight PMMA.[20]

Examination of TG–MS results for PHEMA/salt mixtures revealed that the effects of the salts were primarily manifested in two ways. First, a reaction between PHEMA and alkali halides produced carboxylic acid salts in the polymer residues and resulted in alkyl halide evolution. Second, interactions between ionic salts and ester moieties catalyzed ester decomposition reactions.

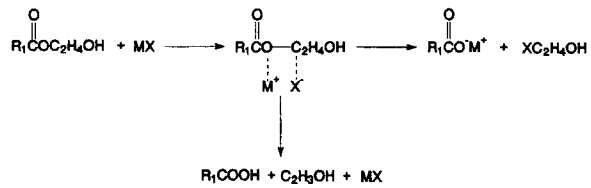

Table III lists the temperatures at which ions that were selective for ethenol (m/z 44), ethylene glycol (m/z 62), and methacrylic acid (m/z 86) maximized during TG–MS analyses of neat PHEMA and PHEMA/salt mixtures. The alkali iodides and CsF had the greatest catalytic effects on ethenol formation. Of all of the salts examined in this study, LiI exhibited the most significant effect on PHEMA decomposition. LiI caused the maximum ethenol evolution temperature to shift from 422°C for neat PHEMA to 229°C for the PHEMA/LiI mixture. Much smaller temperature shifts resulted from the presence of alkali bromides, alkali chlorides, and LiF. The crosslinking reaction between two PHEMA pendant groups to form ethylene glycol was also catalyzed to some extent by all of the salts. Like the ester decomposition pathway, the alkali iodides and CsF exhibited the greatest effects on this reaction with LiI exhibiting the highest catalytic activity.

TG–MS results contained in Table III indicate that methacrylic acid evolution from PHEMA was also affected by the alkali halides. Compared to the results obtained for neat PHEMA, the temperatures corresponding to the maximum rates of methacrylic acid evolution for mixtures containing NaI, KI, CsI, and CsF were significantly lower. Methacrylic acid was not detected by TG–MS analysis of the PHEMA/LiI sample. Maximum evolution rate temperatures for mixtures containing alkali bromides and chlorides were slightly higher than that for neat PHEMA. The maximum evolution rate

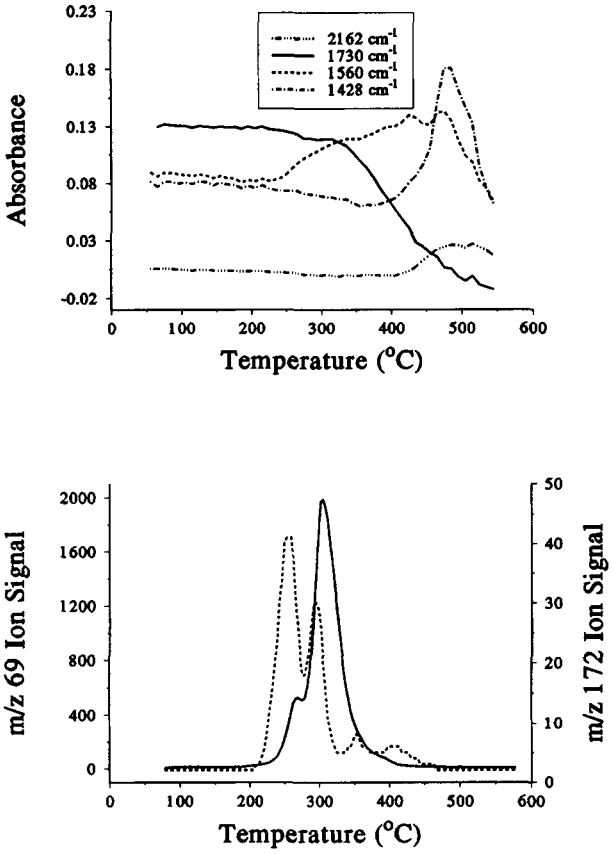

Figure 7 Infrared absorbance band intensity temperature profiles (top) and ion signal temperature profiles (bottom) for m/z 69 (solid line) and m/z 172 (dashed line) obtained by VT-DRIFTS and TG-MS analysis of a PHEMA/NaI mixture.

temperature for the PHEMA/LiF mixture was about the same as that for neat PHEMA. With the exception of the PHEMA/LiI sample, the alkali iodides and CsF were the most effective salts for catalyzing reactions that resulted in methacrylic acid evolution.

Most polymer/salt VT-DRIFTS spectra acquired above 400°C contained carbonate absorbance bands and a small but sharp absorbance band between 2100 and 2200 cm^{-1}. This 2100–2200 cm^{-1} band was likely due to carbon monoxide adsorbed on salt surfaces. Carbonate and CO can be formed by decomposition of carboxylate species.

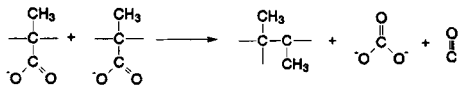

Table IV lists the infrared vibration frequencies for carbon monoxide adsorbed on the salts. The CO

Table III PHEMA/Salt TG-MS Ion Signal Maxima for Selected Ions

	Peak Maximum (°C)		
Salt	Ethenol[a]	Ethylene Glycol[b]	Methacrylic Acid[c]
NEAT	422	379	404
LiI	229	258	—
NaI	364	283	316
KI	389	280	390
CsI	389	293	389
NaBr	415	302	412
KBr	413	305	409
NaCl	415	323	411
KCl	415	312	411
LiF	419	348	405
CsF	371	263	375

[a] From m/z 44 ion signal temperature profile.
[b] From m/z 62 ion signal temperature profile.
[c] From m/z 86 ion signal temperature profile.

absorbance band was not detected in VT-DRIFTS spectra for polymers mixed with LiI and LiF or in spectra derived from PMMA mixed with NaCl and KCl. However, some clear trends in the frequencies of the CO vibration were observed for the other polymer/salt mixtures. Although the CO vibration frequency measured for the PHEMA/CsI sample was about the same as that for gas phase CO, the frequency for this band was greater than the gas phase frequency for all of the other polymer/salt mixtures. The increased CO stretching frequency relative to the gas phase CO vibration is indicative of electron density donation from the CO carbon 5σ

Table IV Infrared Absorbance Band Frequencies (cm^{-1}) for Adsorbed CO

Salt	PMMA	PHEMA
LiI	—	—
NaI	2166	2162
KI	2154	2150
CsI	2145	2143
NaBr	2181	2181
KBr	2162	2162
NaCl	—	2197
KCl	—	2174
LiF	—	—
CsF	2150	2147

orbital,[28-30] which is slightly antibonding, and suggests that CO molecules were adsorbed on alkali cation sites on the salt surface. The frequency of this vibration was found to be dependent on the salt composition rather than the polymer, which is consistent with the assumption that this band was due to CO adsorbed on alkali halide surfaces. For the alkali iodide series, the CO stretching frequency decreased in the order $Na^+ > K^+ > Cs^+$. For salts that contained the same cation (e.g., Na^+ or K^+), the CO vibration frequency decreased as the size of the anion increased ($Cl^- > Br^- > I^-$). This trend may be attributed to increased shielding of salt cations by larger anions, which may weaken interactions between CO and surface cations.

Examination of Table IV reveals that the adsorbed CO VT-DRIFTS band was not detected for either of the polymer/salt mixtures containing lithium. Because alkyl halide and carboxylate species were not detected for the PMMA/LiF sample, it was not surprising that carbon monoxide was not detected for this sample. For the PHEMA/LiF sample, very little alkyl halide and carboxylate were detected, suggesting that the amount of CO formed may have been too small to detect by VT-DRIFTS. However, significant carboxylate and carbonate species were detected for the polymer/LiI mixtures, indicating that CO was generated in large enough quantities to be detected by VT-DRIFTS. Apparently, interactions between CO and LiI were weaker than those for the other alkali halides, permitting CO desorption as soon as it was formed on salt surfaces. The large I^- anion may have effectively shielded the small Li^+ cation, which is only about 60% of the size of Na^+, from significant interactions with carbon monoxide.

CONCLUSIONS

Although no correlations were found that linked the catalytic effects and reactivities of the alkali halides with specific salt properties such as heat of formation, lattice energies, bond dissociation energies, etc., some general trends were detected. For example, the alkali iodides were the most effective for catalyzing polymer decomposition reactions, suggesting that these effects can be attributed primarily to the salt anion rather than to the cation. Heats of formation, bond dissociation energies, and lattice energies of the bromides and chlorides of sodium and potassium are comparable, and the effects of these salts on polymer decomposition were also found to be similar. Samples containing LiF exhibited the least dramatic effects on polymer decompositions. It is probably not a coincidence that LiF has a significantly higher lattice energy than any of the other salts examined in this study. The fact that a dramatic difference was observed between the effects of alkali halides on PMMA and PHEMA suggests that the selection of methacrylic polymer pendant groups may be a critical parameter for the design of polymer binders, particularly when ceramic oxides contain Lewis functionalities that are present at temperatures at which polymer decomposition occurs. The results of the polymer/salt decomposition studies described here suggest that the extent to which carboxylates and carbonates are formed during poly(methacrylate) ceramic binder burnout should be related to the density and strengths of Lewis sites on oxide surfaces. Formation of such species during binder burnout is undesired because excessive temperatures are needed for their removal in nonoxidative sintering environments.

Financial support for this work from Hitachi, Ltd. is gratefully acknowledged.

REFERENCES

1. K. Otsuka, T. Usami, and M. Sekibata, *Yogyo Kyokaishi,* **89,** 309 (1981).
2. K. Otsuka and S. Ogihara, *Yogyo Kyokaishi,* **92,** 210 (1984).
3. K. Otsuka and S. Ogihara, *Yogyo Kyokaishi,* **92,** 629 (1984).
4. K. Otsuka and S. Ogihara, *Yogyo Kyokaishi,* **93,** 28 (1985).
5. H. W. Stetson, *High Technology Ceramics—Past, Present and Future,* Ceramics and Civilization Ser., Vol. 3, American Ceramic Society, Westerville, OH, 1986, p. 307.
6. M. J. Cima and J. A. Lewis, *Ceram. Trans.,* **1,** 567 (1988).
7. Y. N. Sun, M. D. Sacks, and J. W. Williams, *Ceram. Trans.,* **1,** 538 (1988).
8. M. J. Cima, J. A. Lewis, and A. D. Devoe, *J. Am. Ceram. Soc.,* **72,** 1192 (1989).
9. S. Masia, P. D. Calvert, W. E. Rhine, and H. K. Bowen, *J. Mater. Sci.,* **24,** 1907 (1989).
10. R. L. White and A. Nair, *Chem. Mater.,* **2,** 742 (1990).
11. R. L. White and J. Ai, *Chem. Mater.,* **4,** 233 (1992).
12. J. Ai, L. L. Phegley, G. Christen, and R. L. White, *J. Am. Ceram. Soc.,* **78,** 874 (1995).
13. R. L. White, *J. Anal. Appl. Pyr.,* **18,** 269 (1991).
14. R. L. White, *J. Anal. Appl. Pyr.,* **18,** 325 (1991).

15. R. L. White, *Appl. Spectrosc.*, **46,** 1508 (1992).
16. R. L. White, *Anal. Chem.*, **64,** 2010 (1992).
17. R. L. White, *Appl. Spectrosc.*, **47,** 1492 (1993).
18. R. Lin and R. L. White, *Anal. Chem.*, **66,** 2976 (1994).
19. T. Kashiwagi, A. Inaba, J. Brown, K. Hatada, T. Kitayama, and E. Masuda, *Macromolecules,* **19,** 2160 (1986).
20. L. E. Manring, D. Y. Sogah, and G. M. Cohen, *Macromolecules,* **22,** 4654 (1989).
21. P. Cacioli, G. Moad, E. Rizzardo, A. K. Serelis, and D. H. Solomon, *Polym. Bull.*, **11,** 325 (1984).
22. M. S. Choudhary and I. K. Varma, *J. Macromol. Sci.-Chem.*, **A20,** 941 (1983).
23. P. K. Dhal and G. N. Babu, *J. Polym. Sci., Polym. Chem. Ed.*, **22,** 1817 (1984).
24. N. B. Colthup, L. H. Daly, and S. E. Wiberley, *Introduction to Infrared and Raman Spectroscopy,* 3rd ed., Academic Press, New York, 1990.
25. N. Grassie and J. D. Fortune, *Makromol. Chem.*, **168,** 13 (1973).
26. H. H. Adler and P. F. Kerr, *Am. Mineral.*, **47,** 700 (1962).
27. R. L. White and J. Ai, *Appl. Spectrosc.*, **46,** 93 (1992).
28. J. T. Yates, Jr., P. Gelin, and T. Beebe, in *Catalyst Characterization Science,* M. L. Deviney and J. L. Gland, Eds., American Chemical Society, Washington DC, 1985.
29. J. B. Peri, *J. Phys. Chem.*, **72,** 2917 (1968).
30. J. B. Peri, *J. Phys. Chem.*, **86,** 1615 (1982).

Received May 15, 1995
Accepted December 21, 1995